Medical Engineering and Physics 74 (2019) 129–136

Contents lists available at ScienceDirect

Medical Engineering and Physics

journal homepage: www.elsevier.com/locate/medengphy

Multivariate analysis of hemodynamic parameters on intracranial aneurysm initiation of the internal carotid artery

K. Sunderland, J. Jiang*

Michigan Technological University, 1400 Townsend Drive, Houghton, MI, USA

ARTICLE INFO

Article history:
Received 6 September 2018
Revised 30 July 2019
Accepted 8 September 2019

Keywords:
Intracranial aneurysm
Computational fluid dynamics
Hemodynamic stressors
Multivariate predictive modeling

ABSTRACT

Although fluctuating hemodynamic wall stressors are known to impact intracranial aneurysms (IA) initiation, specificity of those stressors has not been evaluated. In this study, using human IA data, we investigated: (1) specificity of stressors in regions with and without IA eventual IA formation; and (2) how combinations of multiple stressors could improve IA formation prediction.

3D computational vasculatures were constructed based on angiographic images of 18 subjects having multiple closely-spaced IAs in the internal carotid artery. Two models were created: Model A with all IAs computationally removed, Model B which kept keep one IA. Computational fluid dynamics (CFD) simulated flow within models. Based on simulated flow fields, wall shear stress and its gradient (WSS, WSSG), oscillatory shear index (OSI), gradient oscillatory number (GON), aneurysm formation index (AFI), and mean number of swirling flow vortices (MV) were analysed. Multivariate logistic regression determined the accuracy of different combinations of those above-mentioned stressors.

Overall, we found that combining hemodynamic stressors improves IA formation prediction over individual indices. Both Model A and Model B's parsimonious model was MV+WSS+GON: AUROC 0.88 and 0.83, respectively. Future studies are planned to understand biological meanings induced by fluctuating stressors.

1. Introduction

Intracranial aneurysms (IA) are pathologic, bulbous expansions of the cerebral arterial wall. These lesions impact an estimated 3–5% of the world population [1] and carry a high degree of morbidity and mortality upon rupture. Among patients with IAs, 15–35% of them present with multiple IAs [2,3]. While conditions triggering IA initiation remain under investigation [4–6], complex vascular hemodynamics is thought to play a significant role [7,8]. Increasing evidence points to inflammation as a leading factor in IA pathogenesis; many inflammatory processes are induced in part by hemodynamic insults [4].

Among hemodynamic indices, wall shear stress (WSS) has a history associated with vascular remodeling, including IA initiation [9–13]. Spatial and temporal changes of WSS may affect biological processes occurring in the arterial wall (e.g. endothelial cells), impacting vascular remodeling through mechanotransduction. Several groups have instigated how WSS and its derivatives are correlated with areas of IA initiation. Meng et al. [14] reported that high WSS spatial gradients (WSSG) were linked to IA initiation. Mantha et al. [12] developed a metric known as aneurysm formation index (AFI), associated with changing directionality of WSS vectors, and showed AFI positively correlated with IA initiation in three side-wall IAs. Shimogonya et al. [11] proposed a novel index known as gradient oscillatory number (GON). GON assessed oscillating compression and tension forces in the vessel and was shown to associate with IA initiation. In a later study, Ford et al. [15] applied GON to five side-wall aneurysm cases and found "the association between the GON and the known aneurysm sites can be identified only in four of the five cases." The latter study [15] prompted a follow-up study by Chen et al., in which 22 cases of side-wall IAs were used and the predictability of WSS and its derivatives was systematically investigated to determine predictive strength [16]. They concluded that "locally elevated WSS and GON are highly correlated (20/22 for WSS and 19/22 for GON) to regions of sidewall IA formation, whilst hemodynamic indices

Abbreviations: IA, Intracranaial Aneurysm; CFD, Computational Fluid Dynamics; WSS, Wall Shear Stress; WSSG, Wall Shear Stress Gradient; OSI, Oscillatory Shear Index; GON, Gradient Oscillatory Number; AFI, Aneurysm Formation Index; MV, Mean Number [of] Flow Vortices.

* Corresponding author.
E-mail addresses: kwsunder@mtu.edu (K. Sunderland), jjiang1@mtu.edu (J. Jiang).

https://doi.org/10.1016/j.medengphy.2019.09.010
1350-4533/

associated with oscillating WSS vectors have much lower correlations [16].” However, in the previous two studies [15,16], only the index prevalence in IA areas was evaluated. Hemodynamic indices are not wholly specific IA areas, appearing in vasculature sections where no (known) IAs occur. Limited specificity may reduce single index’s effectiveness to predict IA initiation, generate false positives, and could account for study inconsistencies [11,12,17].

In this study, an index was added to assess the gross flow complexity within the vessel: analysis of recirculating hemodynamic flow (vortices), and its implications on IA development were investigated. It is worth noting that hemodynamic indices mentioned above for predicting the IA development in the literature are all related to WSS. These indices only assess hemodynamic alterations at the near vessel wall locale. Although their use can be justified from the perspective of mechano-transduction, they give limited insight into broader hemodynamic patterns occurring within the vasculature. Broader hemodynamic patterns occurring within the vasculature, which may also influence IA formation, have not been explicitly investigated. In this sense, this study is exploring a new avenue since how the overall hemodynamics may influence prediction models of IA development as a hypothesis is limited. There is mounting evidence showing that flow vortices are biologically relevant to the IA development, particularly through altering vascular endothelial cells. [7,14,18] More specifically, vortices result in broad-scale alterations flow directionality in relation to laminar flow, changing endothelial cell alignment [19,20] and phenotypic expression [21,22] leading to possible pathological changes in the vasculature. Additionally, reattachment points (points where swirling flow and laminar flow meet) may promote monocyte adhesion on vascular endothelial cells, impacting vascular inflammation and triggering pathologies [23]. In short, we envision that the inclusion of the index derived from flow swirling vortices may provide new information that cannot be quantified by near-wall metrics such as WSSG, AFI, GON, and OSI.

Toward this end, the objectives of our study were twofold. First, the intensity of hemodynamic indices in areas of IA initiation as well as in areas of no IAs were investigated. The second objective, to determine whether or not a combination of multiple hemodynamic indices improve the accuracy of predicting IA initiation. Clinical data containing multiple closely-spaced side-wall IAs located at the Internal Carotid Artery (ICA) were used so that multiple (2–4) IA sites can be identified in the same patient. To our knowledge, minimal work has been done in predicting initiation of multiple ICA located IAs. Recall that vascular pathologies may alter hemodynamics [24]. Consequently, the initial formation of one IA disturbs localized flow and may impact subsequent IA initiation. This was considered an additional contribution of this study. Since pre-aneurysm vascular geometries are scarce, a published computational geometry-based surface reconstruction method [15] was adopted to recreate pre-aneurysm geometries. Simulated flow data were used to assess hemodynamic indices and vortices under the “pre-aneurysm” state. Flow in and around sites of IA formation was simulated using these pre-aneurysm geometries in conjunction with “patient-specific” computational fluid dynamics (CFD) simulations. Our computational approach was methodologically similar to the two aforementioned studies [15,16].

2. Materials and methods

Eighteen subjects with multiple multiple closely-spaced side-wall IAs located within the supra-clinoid segment of the ICA were identified from an internal database aggregating data from the University of Wisconsin and Changhai Hospital (China). This study was exempted by Michigan Technological University’s institutional review board (IRB) as it was a secondary analysis of existing data sets.

2.1. Creation of vascular models

For each subject, 3D-DSA data obtained from standard clinical equipment were loaded into a commercial software package (Mimics Innovation suite V.17, Materialise Inc. Leuven, Belgium) for image segmentation. Particularly, an intensity-based image segmentation method generated vessel geometries. Details of image segmentation protocol can be found in a prior publication [25]. From obtained geometries, 2 groups of models were created: one with all IAs computationally removed from the vessel (Model A), and one with one IA intact (Model B). When Model B contained tandem IAs (distinct separation of IA ostia along the longitudinal axis of the parent vessel), the first (proximal) IA was kept intact, making an assumption that the second (distal) will not affect the hemodynamics upstream of the IA. When IAs were adjacent (two or more IAs opposite each other on the transverse axis of the parent vessel) multiple Model Bs were generated, each with one of their tandem IAs intact.

To create Model A, the following process was used. First, a semi-automated IA removal method [15], implemented in the Vascular Modeling Toolkit (VMTK, V.1.2; http://www.vmtk.org), removed all IAs and reconstructed the IA-free vessel geometry. Next, the IA-free geometry was imported into a commercial mesh editing software (3-Matic V.10, Materialize Inc., Leuven, Belgium) and the geometry was projected onto the original geometry to remove unintended alterations to parent vessel curvature. Geometries were then smoothed to remove surface irregularities. For Model B creation, the 3-Matic software was used to re-attach one IA back onto a copy of the Model A vasculature. An example of an original vessel (all IAs intact) and the result of Models A and B creation can be seen in Fig. 1. Additional examples of vessel reconstruction can be seen in the supplementary material.

To ensure changes in prediction model outcomes between Model A and Model B were due to the remaining IA (Model B) altering flow characteristics, and not simply from one of the ROIs no longer being analyzed, a secondary analysis of Model A data was performed. The secondary analysis of Model A was performed by excluding the ROIs coinciding with the area(s) of reattached IAs (Model B), and assessing their impact on prediction model outcomes.

All models were converted into an unstructured, 3D, volumetric mesh using the open-source mesh generator Tetgen (V1.4.2) [26]. Meshing was driven by an in-house Python script implemented through VMTK. Approximately, 1.5 million computing cells were used per case, with an approximate cell volume of 0.003 mm^3.

2.2. CFD simulation

Blood flow velocity and WSS within the models were calculated using the ANSYS-FLUENT software (v17.0 ANSYS-FLUENT Inc., Lebanon, NH) by numerically solving the Navier–Stokes Equations. Blood was modeled as an incompressible, Newtonian fluid with a dynamic viscosity of 0.004 Pa s, and 1050 kg/m^3 mass density. Rigid walls with a no-slip boundary condition were assumed. An averaged pulsatile flow waveform, taken from Gwilliam et. al., based on magnetic resonance measurements at the internal carotid artery (ICA) of healthy patients was used as the inlet boundary condition [27]. All computational fluid dynamic (CFD) simulations had their flow waveform scaled to the vessel’s inlet cross-sectional area, standardizing the mean volumetric flow rate to 280mL/min. A zero-pressure boundary condition was used for all outlets. The Semi-Implicit Method for Pressure-Linked Equations (SIMPLE) algorithm [28] with a first-order streamline-upwind stabilization approach was used for simulations. The solution for simulations was advanced in time using a fully implicit first-order scheme. Four cardiac cycles were simulated with 1000 time-steps per

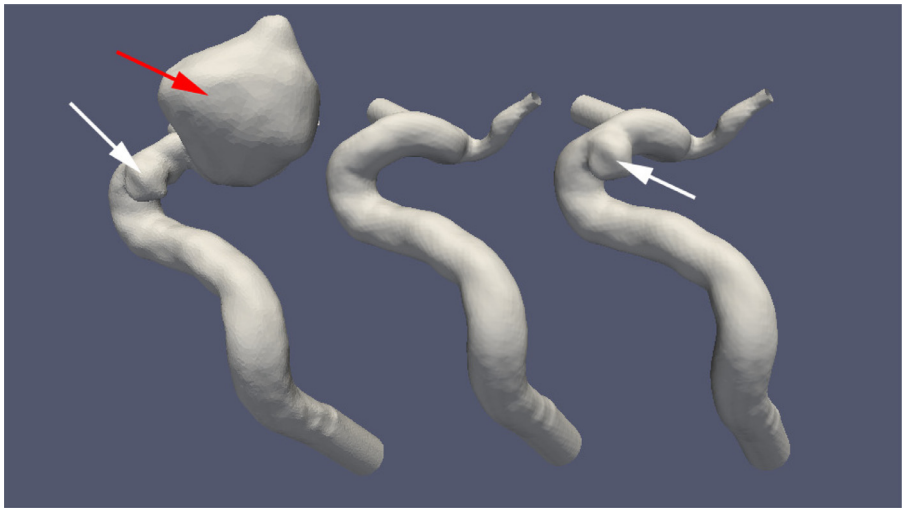

Fig. 1. Vascular model with all IAs intact (left), both IAs computationally removed (center) and 1 IA reattached (right). White arrows identifying the reattached proximal IA, red identifying the distal IA. (For interpretation of the references to colour in this figure legend, the reader is referred to the web version of this article.)

cardiac cycle (time step size = 0.001 second). Twenty equally-spaced time points were saved from the final cardiac cycle for data processing and analysis.

2.3. Calculation of hemodynamic indices

The following hemodynamic parameters, thought as predictive indices for the IA initiation, were calculated from simulated flow: WSS, WSSG), Oscillatory Shear Index (OSI) [29], AFI [12], GON [11], and Mean Number of Flow Vortices [30].

WSS parameters. Tangential, frictional stress caused by blood flowing along the vessel wall is known as WSS. The ANSYS-FLUENT software calculates WSS by the normal velocity gradient at the vessel wall:

$$\tau_w = \mu \frac{\partial v}{\partial n} \tag{1}$$

where μ is the dynamic viscosity. WSS between 1.5–2.5 Pa is known to regulate endothelial structure, function, and gene expression. *In-vivo* and *in-vitro* studies point to elevated WSS values (3.5–28.4 Pa) altering vascular cells, which may impact aneurysm initiation: elastic lamina degradation, proliferation of endothelial cells, and cellular apoptosis [10,31,32].

The calculation of WSSG was similar to methods used in the literature [11,33]. We assume that the vessel wall is represented by a set of surface triangles. Given an arbitrary triangle whose surface normal is n, τ is a function of WSS, locally resides in a plane perpendicular to n. Mathematically, two orthogonal vectors p and q lie within the plane can be constructed as follows: p is the flow direction at time t and q is perpendicular to p and n. Thus, the WSSG is computed by taking local derivatives of the WSS magnitude over the p and q directions for a given time instant t [33]:

$$WSSG = \sqrt{\left(\frac{\partial \tau_p}{\partial p}\right)^2 + \left(\frac{\partial \tau_q}{\partial q}\right)^2}$$
$$\frac{\partial \tau_p}{\partial p} = \nabla\tau \cdot \alpha, \frac{\partial \tau_q}{\partial q} = \nabla\tau \cdot p, p = \frac{\tau}{|\tau|}, q = n \times p \tag{2}$$

where gradient operator ∇ denotes partial derivatives of the magnitude of τ in its coordinate directions.

If the flow direction p in Eq. (2) becomes an average flow direction over the cardiac cycle, the instantaneous spatial vector of WSS, namely $G = (\frac{\partial \tau_p}{\partial p}, \frac{\partial \tau_q}{\partial q})$, can be used to calculate the GON metric, which reflects oscillations in the directionality of spatial gradients of WSS over the cardiac cycle [11].

The GON metric can be evaluated as follows [11],

$$GON = 1 - \frac{|\int_0^T G dt|}{\int_0^T |G| dt} (0 \le GON \le 1) \tag{3}$$

where T is the cardiac cycle.

Oscillatory shear index. OSI is a non-dimensional parameter, computing oscillations in the direction of the WSS vectors over the course of a cardiac cycle:

$$OSI = \frac{1}{2}\left\{1 - \frac{|\int_0^T \tau_i dt|}{\int_0^T |\tau_i| dt}\right\} \tag{4}$$

were τ_i represents the WSS vector at a given time step across the duration of the cardiac cycle (T). The OSI is changes to WSS vector alignment with the cardiac cycle's temporally-averaged WSS vector. An OSI of 0 indicates no change in directionality and 0.5 being a complete direction reversal.

Aneurysm formation indicator. The AFI [12] quantifies the variation in angle between the instantaneous WSS vector and time-averaged WSS vector:

$$AFI = cos(\theta) = \frac{\tau_i \cdot \tau_{av}}{|\tau_i| * |\tau_{av}|} \tag{5}$$

For each point along the vessel wall, the minimum AFI calculated during the cardiac cycle was used to indicate the greatest deviation of the WSS vector from its mean direction. A minimum AFI of −1, 0, and 1 indicate deviations of 180°, 90°, and 0° respectively.

Number of flow vortices. Areas of recirculating hemodynamic flow (vortices) have been used to assess vessel spatial flow complexity and temporal flow stability [30,34,35]. Identification of vortices was performed for all 20 time-steps of the analysed data, and identified vortices were mapped to 3D surface structures (*iso-surfaces*). The mean number of vortices was calculated by counting the number of disconnected *iso-surfaces* and taking their average over the cardiac cycle. Details of the identification and mapping of vortices are explained in our previous publication [36].

The spatially averaged value of aforementioned indices was identified within the areas of eventual IA initiation as well as in ROIs with no known IA initiation. ROIs with no IA initiation acted as a negative control for statistical predictive modeling, strengthening prediction accuracy. An example of elevated indices within areas of IA initiation can be seen in Fig. 2(a) and (b) showing IA areas with reduced calculated indices.

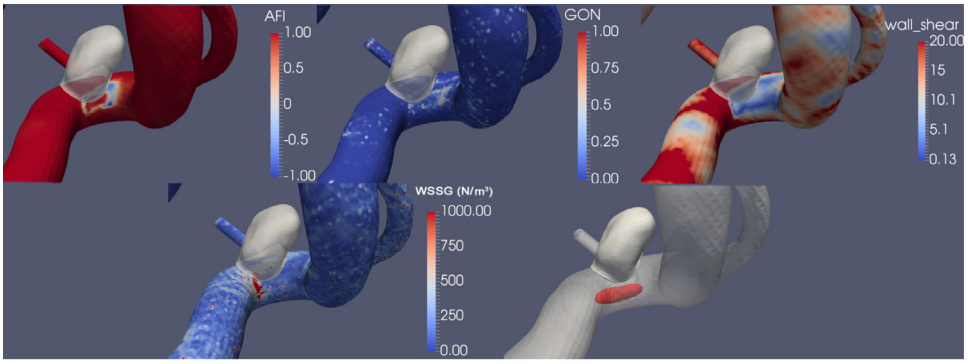

(a) Elevated indices at IA sites

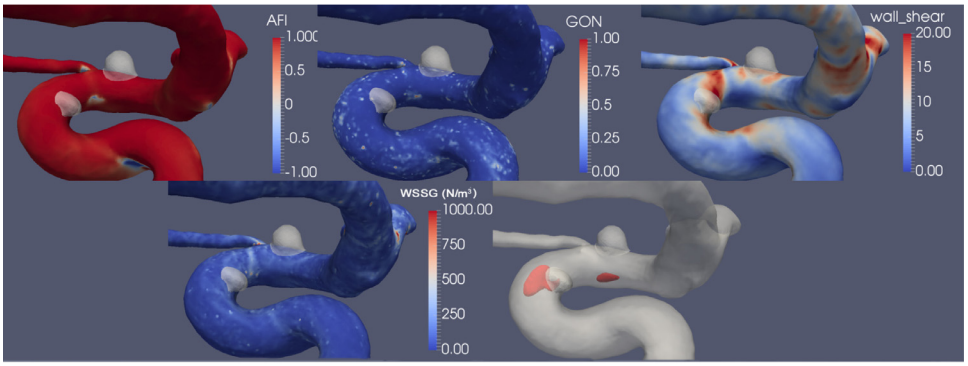

(b) Reduced indices at IA sites

Fig. 2. Simulated flow showing elevated hemodynamic indices (or reduced AFI) [top] or reduced indices (or increased AFI) [bottom] at areas of IA initiation: AFI, GON, WSS, WSSG. An identified vortex did occur within one (of two) sites of IA initiation. (For interpretation of the colour in this figure, the reader is referred to the web version of this article.)

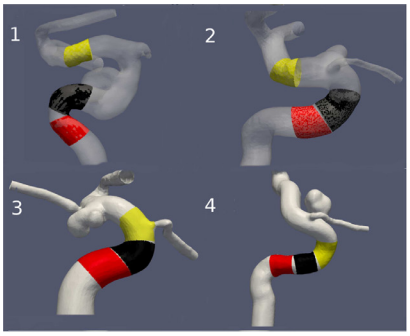

(a) Non-IA ROIs.

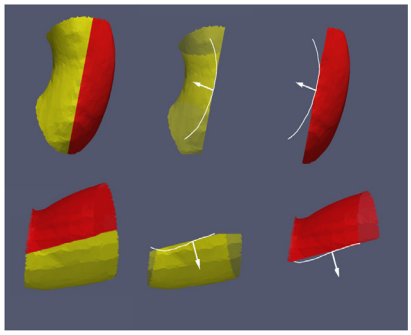

(b) Non-IA ROI division.

Fig. 3. (a) Examples of non-IA ROIs. (1) and (2): two ROIs proximal to the first IA and one distal to the last area of IA development. (3) and (4): three ROIs proximal to the first IA. (b) ROI division in relation to the vessel Frenet Frame normal (yellow) and opposite the Frenet Frame normal (red). White line is the vessel curvature and arrow pointing to normal. (For interpretation of the references to color in this figure legend, the reader is referred to the web version of this article.)

2.4. Regions of interest

For areas containing IA sites, ROIs of vessel segments spanning the area(s) of the removed IA's ostium were chosen. For ROIs of non-IA initiation, three vessel segments for each patient case were chosen. The length of each non-IA ROI equals the cross-sectional diameter of their parent vessel (proximal to the first identified IA). Two non-IA ROIs were chosen in tandem, proximal to the site of the first formed IA, while the third was chosen distal to the site of the distal-most IA (Fig. 3(a)). In the event that the third ROI encountered the parent vessel bifurcation, it was instead chosen directly proximal to the first two ROIs (Fig. 3(a)). All non-IA ROIs were divided laterally, and each side investigated individually as stressors are not uniform around the wall of the entire vessel [37]. The division plane for non-IA ROIs was selected in relation to the Frenet Frame normal of the vessel centerline tangent [38]. The Frenet normal, defining the oscillating plane of the centerline curvature, at the midpoint of each ROI centerline was chosen for respective cut planes. (Fig. 3(b)).

2.5. Statistical analysis

The mean values of WSS, WSSG, OSI, GON, and AFI along the ROIs and flow vortices were determined within all ROIs. Correlation amongst hemodynamic variables was performed to eliminate redundant variables and over-fitting in predictive modeling. Multi-

Table 1
Pearson's correlation coefficient (r) (and *p*-value) of mean of hemodynamic variables within all ROIs to the occurrence of an IA: Model A and Model B data.

Variable	r : p-value	Variable	r : p-value
Model A		Model B	
AFI	−0.190 : 0.022	AFI	−0.170 : 0.021
WSS	0.333 : < 0.001	WSS	0.309 : < 0.001
WSSG	0.241 : 0.004	WSSG	0.177 : 0.016
GON	0.221 : 0.008	GON	0.207 : 0.005
Flow vortex	0.477 : < 0.001	Flow vortex	0.381 : < 0.001

variate logistic regression analysis (step-wise elimination) was performed to identify index combinations significant in predicting IA initiation. Model B was assessed separately from IA-free models (Model A). Using Model B, how the presence of one proximal IA impacts predictive outcomes was evaluated [39].

The model(s) derived from multivariate logistic regression were tested using repeated k-fold cross-validation (10 folds, 10 repeats). The area under the receiver operating characteristic curve (AUROC) assessed accuracy of grouped indices to predict IA initiation. An identical analysis was performed on each variable individually and their AUROC assessed alongside the grouped characteristic predictions. Statistical analyses were performed using the R (Version 3.4.4)[1] and its integrated environment (RStudio statistical platform, Version 1.0.143).[2]

3. Results

Pearsons correlation analysis among study indices showed AFI and OSI as highly correlated ($r = 0.92$, $p < 0.001$). These indices relate alterations of WSS vector directionality, giving grounds for their correlation. OSI was removed from subsequent analysis.

Additionally, the correlation of spatial means of hemodynamic indices to the occurrence of an IA within all analyzed ROIs can be seen in Table 1. This lack of strong correlative relation of IA development to hemodynamic indices indicates the need of combined parameters in order to improve the IA prediction.

Step-wise multivariate logistic regression identified the index combination best suited (from available data) to identify areas of IA initiation. In Model A, combining mean number of vortices (MV), WSS and GON acted as the strongest parsimonious model for predicting IA formation. It is worth noting, mean GON values were found to be highly right-skewed, with small mean values. The natural log transform of GON (LNGON) means was taken to help the GON values conform to normality for analysis and lower its weight on odds ratios in relation to other indices. The odds ratio(s) (Eq. (6)) of the chosen hemodynamic indices show that the occurrence of flow vortices increases the odds of the IA initiation by 14.34 times, LNGON increases the odds by 6.45 times, and elevated WSS increases odds by 1.33 times.

$$Odd_{NoIA} = exp^{2.66*MV+1.864*GON+0.286*WSS+0.938} \quad (6)$$

Repeated k-fold cross-validation with the combined MV+GON+WSS model compared against individual indices were used to assess the combined model's predictive strength. The combined predictive model showed stronger predictive accuracy (AUROC 0.879, 95% CI 0.821 – 0.942) over any individual index.

A similar analysis was performed on Model B data, assuming development of the attached IA impacted subsequent flow characteristics in areas of distal IA formation. Model B's analysis determined the combination of MV+WSSG+LNGON indices still created the parsimonious model, yet the impact of each index was altered. K-fold cross-validation of Model B data, using Model A indices (MV+WSS+LNGON), showed a slight reduction in predictive accuracy: AUROC 0.879 and 0.824 (CI 0.737 – 0.912) for Model A and B, respectively. Yet this change is difficult to conclude due to the overlapping value of each Model's AUC confidence intervals (CI). Fig. 4 shows the ROC and the AUROC for Model A and Model B analysis. The odds ratio for Model B based on the MV+WSS+LNGON prediction was:

$$Odd_{1IA_{MV+WSS+LNGON}} = exp^{1.789*MV+1.69*GON+0.219*WSS+0.888} \quad (7)$$

To assess if changes in index strength for Model B data arose from one of the IA ROIs no longer being analyzed, or from Model B's remaining IA altering flow characteristics, a secondary analysis of Model A data was performed. ROIs coinciding with the area(s) of IA reattachment (in Model B) were excluded from Model A data, and the impact on predictive outcomes was assessed. K-fold cross validation with the MV+WSS+LNGON predictive model was performed for the secondary analysis of Model A data. Outcomes of the secondary analysis showed similar predictive outcomes to Model A's original analysis: AUROC of 0.883 (CI: 0.806 – 0.958) and 0.879, respectively. Yet the strength of LNGON marking an almost 2 fold increase in its odds ratio: 6.45–11.665 original vs secondary analysis, respectively. Table 2 shows the odds ratios of indices under differing analyses.

Table 2
Odds ratios of predictive indices for the analysis of Model A (A1), secondary analysis of Model A (A2), and Model B data (B). Analysis was performed with the MV+LNGON+WSS indices in predictive models. Values in bold indicating marked differences in index strength in relation to the A1 Model.

Model	MV	LNGON	WSS
A1	14.34	6.45	1.33
A2	10.49	**11.67**	1.39
B	**5.98**	5.42	1.25

4. Discussion

Evidence points to disturbed blood flow impacting endothelial cell morphological changes and subsequent vascular remodeling, such as the formation of IAs [18]. Indices assessing hemodynamic conditions have been developed and correlated with areas of IA formation, however, these are all WSS-based [9–13]. In this study, we attempted to add an additional hemodynamic index related to (flow) vortices to better depict flow disturbance within the vasculature, thereby improving the prediction of IA initiation. Furthermore, gaps lie between predictive analyses performed in studies available in the literature [12,15,16], as chosen indices are often individually correlated only with areas of known IA development. This study demonstrated that a multiple-index approach to IA development may be of strong benefit to predictive accuracy. It is worth nothing that additional hemodynamic indices may be of additional interest toward IA development. Additional indices were not included as to not detract from our intended purpose of highlighting the need for a multiple-index approach, and the importance of assessing flow vortices in IA development. Collectively, this study improved our understanding of IA formation prediction.

The elevation or reduction in hemodynamic indices in this study was not wholly specific to areas of IA formation, arising in many areas with no IA initiation. This observation stresses the importance of adopting a multivariate approach to predictive modeling. Our preliminary results demonstrated that combinations of hemodynamic variables improved the accuracy of predicting the IA formation, as indicated by the elevated AUROC in relation to individual indices. Combining the assessment of WSS, LNGON and

[1] https://www.r-project.org/.
[2] https://www.rstudio.com/.

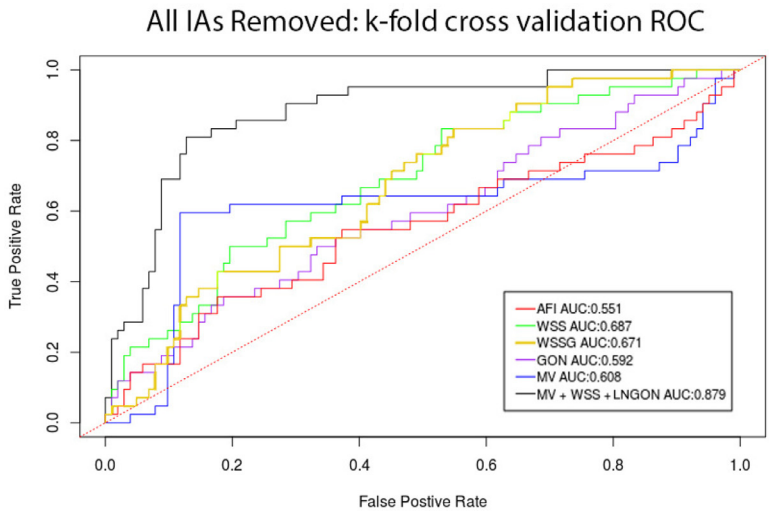

(a) Model A

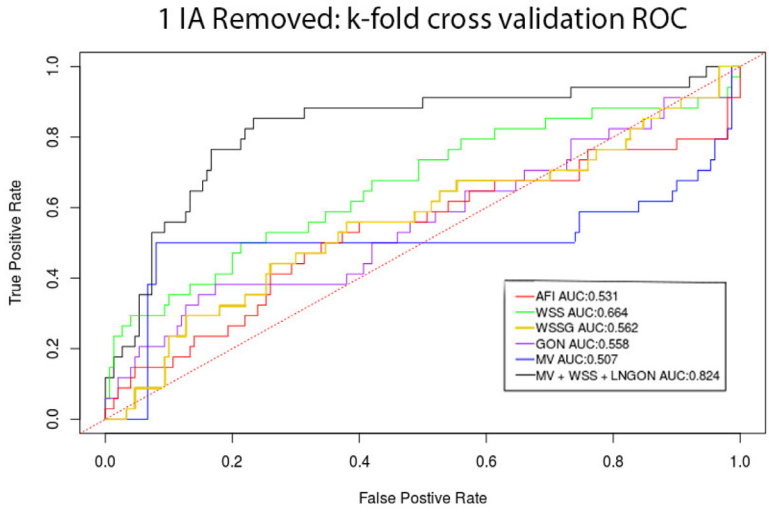

(b) Model B

Fig. 4. ROC curves of averaged prediction probabilities from repeated k-fold cross-validation of regression modeling. The AUROC values of individual indices were assessed (AFI, WSS, WSSG, LNGON, and MV) as well as the parsimonious combined model (MV+WSS+GON). (a) Model A, (b) Model B. (For interpretation of the colour in this figure, the reader is referred to the web version of this article.)

MV (mean number of vortices) generated the strongest predictive model based on data investigated. The adoption of these indices into a predictive model is supported by ideas that alterations in flow patterns and increasing shear stress impact vascular endothelial cells [21], and could impact IA initiation [40]. On the other hand, the hemodynamic variables are only assessed with a present state of IA development. Additional IAs in subjects may have initiated in the future. In order to further validate predictive models, a long-term longitudinal study should be conducted.

While all Models show that MV, LNGON, and elevated WSS pay a significant role in the prediction of IA initiation, the impact that each individual index had on the ability to predict IA initiation varied between Models. In our study, an almost two fold increase in LNGON's impact was seen between Model A and its secondary analysis. As no equivalent increase in LNGON strength was seen in Model B analysis, it suggests that localized altered flow conditions (in the first IA ROI) may have triggered additional alterations in downstream vascular locales. This observation makes a physical sense because the presence of an IA influences the downstream flow disturbance and the opposite is not true. One limitation of this study is that the order of temporal occurrence for IAs was unknown. Otherwise, more insight would be provided.

The presence of a singular IA has also been shown to alter the localized hemodynamics [36] and such changes may also propagate downstream in the vasculature. An evaluation of Model B (one IA intact) data showed that while the alteration to the localized flow did not change the indices needed for the prediction model, it changed hemodynamic conditions and impacted the predictive strength of each index, especially when compared with the secondary analysis of Model A. The introduction of one IA into the vasculature altered local flow conditions, reducing the odds ratio of both vortices (10.49–5.98) and LNGON (11.66–5.42) on IA prediction.

It is important to note that simulation conditions could alter prediction outcomes. Additional simulations were run using four (4) randomly selected cases with the following modifications: a differing waveform representative among older patients (age 68 ± 8 years) by Hoi et al. [41], higher mesh density (6 million computa-

tional cells), and higher sampling rate (40 steps saved across final cardiac cycle). Changes to hemodynamic indices were assessed between, the original simulation conditions (Gwilliam waveform, 20 time-steps per cardiac cycle, ~1.5 million computational cells) and higher (~6 million) mesh density, increased sampling rate from 20 to 40 time-steps per cardiac cycle, and Gwilliam vs Hoi waveform at 20 time-steps per cardiac cycle with ~1.5 million cell mesh density. Visual comparison between simulation conditions and resultant indices can be seen in the supplementary material (Fig. S3). The mean value of indices in ROIs was compared between the different simulation conditions using paired *t*-tests. Table ST1 in the supplemental material shows the outcome of *t*-test and the average percent change in variables under separate simulation conditions. Additional information on the assessment of hemodynamic indices and vortices between differing simulation conditions can be seen in the supplementary material.

In summary, our supplementary observations showed that, of the different simulation conditions, inlet waveform was shown to have the largest impact on the intensity of hemodynamic indices in assessed ROIs. While varied index intensity would impart changes to model odds ratios, the overall patterns of high and low hemodynamics indices between ROIs were maintained between waveforms. The maintenance of high and low indice patterns would, in theory, help maintain chosen indices being used in predictive models. As IA generation is thought to increase as a function of age [42], a larger study using vascular models from patients with known age paired with a "patient-specific" waveform or at least an age-appropriate waveform, may help better understand the impact each index has on predictive models. It would also be worth investigating, on a higher number of cases, the impact that very high mesh density (15–20 million computational cells) may have on better resolving swirling flow patterns [43]. As suggested by Valen-Sendstad and Steinman [44], CFD solution strategies impact simulated hemodynamics, particularly in and around intracranial aneurysms. While this study was not concerned with assessing flow within the IAs themselves, future work may benefit from investigating the consistency of results simulated by different CFD solvers and settings if assessing indices within IAs. Also, mesh density could also play a role in predicting the flow behaviors inside IAs, particularly, the formation of flow vortices [45]. Those remain to be our future work.

While this work has given good insight into the assessment of hemodynamic indices and their ability to predict IA development, this current study is limited by a small pool of human subject and the lack of "patient-specific" flow waveforms. Future studies, particularly, in prospective studies, may benefit by expanding upon our original methodology. Additionally, comparing hemodynamic indices between patients with IAs in the internal carotid artery against patients with no (known) developed IAs could further elucidate the hemodynamic conditions indicative of IA development in a long-term prospective study.

5. Conclusion

IA formation is a multi-faceted vascular pathology, with varying conditions impacting their development [46]. A comprehensive analysis of hemodynamic indices applied to predictive modeling could help elucidate patients at risk for developing an IA while improving the understanding of this vascular pathology. This study suggests that a combination of hemodynamic indices perform better in predicting areas of IA initiation as opposed to relying on individual indices. Increasing wall shear stress intensity and fluctuations, coupled with complex swirling flow patterns indicate area(s) with a higher possibility of IA development. It was noted that the development of an IA changed flow in the localized area, altering expressions of hemodynamic indices. Reassessment of models may be needed to properly identify areas of IA initiation in the presence of differing vascular pathologies: stenosis, severe tortuosity, etc. The consequences from these additional vascular alterations, and how they impact IA initiation, cannot be determined from this work and will require additional investigations.

Declaration of Competing Interest

None.

Acknowledgment

The study was partially funded by a research contract through Siemens Medical Solution (USA) Inc. Kevin Sunderland is currently supported by a pre-doctoral fellowship from the American Heart Association [18PRE33990321]. No funding sources had any role in the collection, analysis, or interpretation of study data. We also thank our colleagues, particularly, Dr. Charles Strother (University of Wisconsin) and Dr. Qinghai Huang (Changhai Hospital, Shanghai, China) for providing us some data used in this study.

This study is a secondary analysis of existing human subject data. The Institutional Review Board at the Michigan Technological University has granted an exemption for this study under the US National Institutes of Health Exemption #4.

Supplementary material

Supplementary material associated with this article can be found, in the online version, at doi:10.1016/j.medengphy.2019.09.010.

References

[1] Vlak MH, ALgra A, Brandenburg R, Rinkel GJ. Prevalence of unruptured intracranaial aneurysms, with emphasis on sex, age, comorbidity, country, and time period: a systematic review and meta-analysis. Lancet Neurol 2011;10(7):626–36.
[2] Kaminogo M, Yonekura M, Shibata S. Incidence and outcome of multiple intracranial aneurysms in a defined population. Stroke 2003;34(1):16–21.
[3] Ellamushi HE, Grieve JP, Jager HR, Kitchen ND. Risk factors for the formation of multiple intracranial aneurysms. J Neurosurg 2001;94(5):728–32.
[4] Chalouhi N, Hoh BL, Hasan D. Review of cerebral aneurysm formation, growth, and rupture. Stroke 2013;44(12):3613–22.
[5] Starke RM, Raper DM, Ding D, Chalouhi N, Owens GK, Hasan DM, et al. Tumor necrosis factor-α modulates cerebral aneurysm formation and rupture. Transl Stroke Res 2014;5(2):269–77.
[6] Juvela S. Natural history of unruptured intracranial aneurysms: risks for aneurysm formation, growth, and rupture. In: New Trends in Cerebral Aneurysm Management. Springer; 2002. p. 27–30.
[7] Sforza DM, Putman CM, Cebral JR. Hemodynamics of cerebral aneurysms. Ann Rev Fluid Mech 2009;41:91–107.
[8] Lasheras JC. The biomechanics of arterial aneurysms. Ann Rev Fluid Mech 2007;39:293–319.
[9] Rossitti S. Shear stress in cerebral arteries carrying saccular aneurysms: a preliminary study. Acta Radiol 1998;39(6):711–17.
[10] Meng H, Tutino V, Xiang J, Siddiqui A. High WSS or low WSS? complex interactions of hemodynamics with intracranial aneurysm initiation, growth, and rupture: toward a unifying hypothesis. Am J Neuroradiol 2014;35(7):1254–62.
[11] Shimogonya Y, Ishikawa T, Imai Y, Matsuki N, Yamaguchi T. A realistic simulation of saccular cerebral aneurysm formation: focussing on a novel haemodynamic index, the gradient oscillatory number. Int J Comput Fluid Dyn 2009;23(8):583–93.
[12] Mantha A, Karmonik C, Benndorf G, Strother C, Metcalfe R. Hemodynamics in a cerebral artery before and after the formation of an aneurysm. Am J Neuroradiol 2006;27(5):1113–18.
[13] Geers AJ, Morales HG, Larrabide I, Butakoff C, Bijlenga P, Frangi AF. Wall shear stress at the initiation site of cerebral aneurysms. Biomech Model Mechanobiol 2017;16(1):97–115.
[14] Meng H, Wang Z, Hoi Y, Gao L, Metaxa E, Swartz DD, et al. Complex hemodynamics at the apex of an arterial bifurcation induces vascular remodeling resembling cerebral aneurysm initiation. Stroke 2007;38(6):1924–31.
[15] Ford M, Hoi Y, Piccinelli M, Antiga L, Steinman D. An objective approach to digital removal of saccular aneurysms: technique and applications. Br J Radiol 2009;82(special_issue_1):S55–61.
[16] Chen H, Selimovic A, Thompson H, Chiarini A, Penrose J, Ventikos Y, et al. Investigating the influence of haemodynamic stimuli on intracranial aneurysm inception. Ann Biomed Eng 2013;41(7):1492–504.

[17] Kulcsar Z, Ugron A, MarosfHoi M, Berentei Z, Paal G, Szikora I. Hemodynamics of cerebral aneurysm initiation: the role of wall shear stress and spatial wall shear stress gradient. Am J Neuroradiol 2011;32(3):587–94.
[18] Chiu J-J, Chien S. Effects of disturbed flow on vascular endothelium: pathophysiological basis and clinical perspectives. Physiol Rev 2011;91(1):327–87.
[19] Chiu J-J, Wang D, Chien S, Skalak R, Usami S. Effects of disturbed flow on endothelial cells. J Biomechl Eng 1998;120(1):2–8.
[20] Balaguru UM, Sundaresan L, Manivannan J, Majunathan R, Mani K, Swaminathan A, et al. Disturbed flow mediated modulation of shear forces on endothelial plane: a proposed model for studying endothelium around atherosclerotic plaques. Sci Rep 2016;6:27304.
[21] Hahn C, Schwartz MA. Mechanotransduction in vascular physiology and atherogenesis. Nat Rev Mol Cell Biol 2009;10(1):53.
[22] Miao H, Hu Y-L, Shiu Y-T, Yuan S, Zhao Y, Kaunas R, et al. Effects of flow patterns on the localization and expression of ve-cadherin at vascular endothelial cell junctions: in vivo and in vitro investigations. J Vascul Res 2005;42(1):77–89.
[23] Chiu J-J, Chen C-N, Lee P-L, Yang CT, Chuang HS, Chien S, et al. Analysis of the effect of disturbed flow on monocytic adhesion to endothelial cells. J Biomech 2003;36(12):1883–95.
[24] Mannino RG, Myers DR, Ahn B, Wang Y, Rollins M, Gole H, et al. Do-it-yourself in vitro vasculature that recapitulates in vivo geometries for investigating endothelial-blood cell interactions. Sci Rep 2015;5:12401.
[25] Jiang J, Strother C, Johnson K, Baker S, Consigny D, Wieben O, et al. Comparison of blood velocity measurements between ultrasound doppler and accelerated phase-contrast mr angiography in small arteries with disturbed flow. Phys Med Biol 2011;56(6):1755.
[26] Si H. Tetgen, a delaunay-based quality tetrahedral mesh generator. ACM Trans Math Softw 2015;41(2):11:1–11:36.
[27] Gwilliam MN, Hoggard N, Capener D, Singh P, Marzo A, Verma PK, et al. Mr derived volumetric flow rate waveforms at locations within the common carotid, internal carotid, and basilar arteries. J Cerebral Blood Flow Metab 2009;29(12):1975–82.
[28] Patankar S. Numerical Heat Transfer and Fluid Flow, CRC Press; 1 edition (January 1, 1980). https://www.crcpress.com/Numerical-Heat-Transfer-and-Fluid-Flow/Patankar/p/book/9780891165224
[29] He X, Ku D. Pulsatile flow in the human left coronary artery bifurcation: average conditions. J Biomech Eng 1996;118:74–82.
[30] Sunderland K, Haferman C, Chintalapani G, Jiang J. Vortex analysis of intra-aneurismal flow in cerebral aneurysms. Comput Math Methods Med 2016;2016.
[31] Dolan JM, Kolega J, Meng H. High wall shear stress and spatial gradients in vascular pathology: a review. Ann Biomed Eng 2013;41(7):1411–27.
[32] Dolan JM, Meng H, Sim FJ, Kolega J. Differential gene expression by endothelial cells under positive and negative streamwise gradients of high wall shear stress. Am J Physiol Cell Physiol 2013;305(8):C854–66.
[33] Mut F, Lhner R, Chien A, Tateshima S, Viñuela F, Putman C, et al. Computational hemodynamics framework for the analysis of cerebral aneurysms. Int J Numer Methods Biomed Eng 2011;27(6):822–39.
[34] Byrne G, Mut F, Cebral J. Quantifying the large-scale hemodynamics of intracranial aneurysms. Am J Neuroradiol 2014;35(2):333–8.
[35] Oeltze-Jafra S, Cebral JR, Janiga G, Preim B. Cluster analysis of vortical flow in simulations of cerebral aneurysm hemodynamics. IEEE Trans Vis Comput Graph 2016;22(1):757–66.
[36] Sunderland K, Huang Q, Strother C, Jiang J. Two closely-spaced aneurysms of the supraclinoid internal carotid artery: how does one influence the other? J Biomech Eng 2019 [Epub ahead of print]. doi:10.1115/1.4043868.
[37] Lauric A, Hippelheuser J, Safain MG, Malek AM. Curvature effect on hemodynamic conditions at the inner bend of the carotid siphon and its relation to aneurysm formation. J Biomech 2014;47(12):3018–27.
[38] Bullitt E, Gerig G, Pizer SM, Lin W, Aylward SR. Measuring tortuosity of the intracerebral vasculature from MRA images. IEEE Trans Med Imag 2003;22(9):1163–71.
[39] Wermer MJH, van der Schaaf IC, Velthuis BK, Algra A, Buskens E, Rinkel GJE. Follow-up screening after subarachnoid haemorrhage: frequency and determinants of new aneurysms and enlargement of existing aneurysms. Brain 2005;128(10):2421–9.
[40] Uzarski JS, Scott EW, McFetridge PS. Adaptation of endothelial cells to physiologically-modeled, variable shear stress. PloS One 2013;8(2):e57004.
[41] Hoi Y, Wasserman BA, Xie YJ, Najjar SS, Ferruci L, Lakatta EG, et al. Characterization of volumetric flow rate waveforms at the carotid bifurcations of older adults. Physiol Measur 2010;31(3):291.
[42] Backes D, Vergouwen MD, Tiel Groenestege AT, Bor ASE, Velthuis BK, Greving JP, et al. Phases score for prediction of intracranial aneurysm growth. Stroke 2015;46(5):1221–6.
[43] Valen-Sendstad K, Piccinelli M, Steinman DA. High-resolution computational fluid dynamics detects flow instabilities in the carotid siphon: implications for aneurysm initiation and rupture? J Biomech 2014;47(12):3210–16.
[44] Valen-Sendstad K, Steinman DA. Mind the gap: impact of computational fluid dynamics solution strategy on prediction of intracranial aneurysm hemodynamics and rupture status indicators. Am J Neuroradiol 2014;35(3):536–43.
[45] Jain K, Jiang J, Strother C, Mardal K-A. Transitional hemodynamics in intracranial aneurysms-comparative velocity investigations with high resolution lattice boltzmann simulations, normal resolution ansys simulations, and MR imaging. Med Phys 2016;43(11):6186–98.
[46] Signorelli F, Sela S, Gesualdo L, Chevrel S, Tollet F, Pailler-Mattei C, et al. Hemodynamic stress, inflammation, and intracranial aneurysm development and rupture: a systematic review. World Neurosurg 2018;115:234–44.